R.E.M. (Rekayasa Energi Manufaktur) Jurnal | Vol. 11 No.2/2026
ISSN online (2528-3723)
http://doi.org/10.21070/rem.v11i2.1881

The Effect of Combined Circular and Hexagonal Perforation on Multi-Blade Twisted Tape on Thermal-Hydraulic Performance

Bayu Adistia[1], Fahrudin Fahrudin[2*], Nicky Yongkimandalan[3]
*Email corresponding author: fahrudin@upnvj.ac.id

[1, 2, 3]*Department of Mechanical Engineering, Universitas Pembangunan Nasional Veteran Jakarta, 12450, Indonesia*

Article history: Received: 26 August 2026 | Revised: 2 October 2026 | Accepted: 8 October 2026

Abstract*. Twisted tape is a passive method to enhance the thermal hydraulic performance of heat exchangers, but increasing the number of blades in a multi-blade twisted tape (MBTT) can lead to flow blockage and reduce performance at high blade counts. This study evaluates alternating circular-hexagonal perforations on multi-blade twisted tape (MBTT) with 2, 4, 6, and 8 blades at Reynolds numbers of 6,000–22,000 using Computational Fluid Dynamics (CFD). Performance is evaluated based on the Nusselt number, friction factor, pressure drop, and Performance Evaluation Criterion (PEC). The results show a maximum Nusselt number increase of 82.0% on MBTT 6-H at Re=22,000, while a maximum PEC of 1.136 is obtained on MBTT 2-C-H. In the MBTT 8-C-H configuration, the pressure drop reaches 12,246.76 Pa and the PEC decreases to 0.851. The results indicate that circular–hexagonal perforation can maintain an increase in heat transfer at a high number of blades, but the hydraulic penalty becomes more dominant in the eight-blade configuration.*

Keywords *– Multiblade Twisted Tape; Combined Perforation; Nusselt Number; Friction Factor; Performance Evaluation Criterion.*

INTRODUCTION

In modern industrial sectors such as power generation, cooling systems, food processing, petrochemicals, and renewable energy, heat exchangers are vital elements that determine operational success. The optimization of heat transfer methods in these devices is continuously studied in depth because it directly correlates with energy efficiency and operational cost saving [1], [2]. In fluid mechanics, a circular pipe that does not undergo geometric engineering will trigger the formation of a thermal boundary layer in the region near the wall. This layer is responsible for the increased thermal resistance that limits heat transfer efficiency [3]. Most heat exchangers are designed using turbulent flow regimes. This flow is chosen because it can enhance fluid mixing, accelerate heat transfer, and thin the thermal boundary layer, thereby significantly improving thermal efficiency [4].

The insertion of twisted tape into pipes is a popular passive method to enhance the thermal-hydraulic efficiency of heat exchangers in turbulent flow. This geometry induces swirl flow and secondary flow that intensify the mixing of the core and wall fluids. This thins the thermal boundary layer and significantly increases convective heat transfer [5], [6]. The consequence of this high turbulence is an increase in the friction factor and pressure drop in the heat exchanger system. This increased hydraulic resistance forces the system to require higher pumping power compared to pipes without insert structures [7]. The feasibility of using twisted tape must consider the balance between the increase in heat transfer and the pressure drop. This is evaluated through the Performance Evaluation Criterion (PEC). A PEC value > 1 indicates that the increase in heat transfer is more dominant than the increase in pumping power, thus the geometry is considered thermally-hydraulically effective [8].

To trigger a stronger swirl flow effect, design engineering through the increase in the number of blades on the twisted tape (multi-blade twisted tape) has been extensively explored. The insertion of a turbulator with up to 4 blades successfully increased the Nusselt number by 153.32%, although on the other hand, it triggered a consequence in the form of a friction factor spike of up to 630.09% [9] . The four-blade configuration significantly enhanced heat transfer with an average increase in the Nusselt number of 87.84% at Re = 1000. However, this is accompanied by a hydraulic penalty in the form of an increase in the friction factor by up to 136.36% [10]. The addition of excessive blades (such as the 8-blade model) actually reduces thermal performance due to flow blockage. Gaps that are too narrow change the function of the device from a turbulence inducer to a solid flow barrier that hinders fluid convection [11].

The creation of perforation holes on the blade becomes an engineering solution to address flow blockage. Perforation allows some fluid to flow through the blade, thereby reducing pressure drop and friction without sacrificing heat transfer performance. perforation on the classic twisted tape triggers secondary vortex flow that disrupts the thermal boundary layer. Unlike surface interferences such as dimples that increase resistance, perforations loosen the fluid flow, effectively reducing pressure drop and friction factor [12]. The shape of the perforation on the twisted tape has a different effect on the thermal-hydraulic performance. Hexagonal perforations on a single twisted

Copyright © 2026 Author [s]. This is an open-access article distributed under the terms of the Creative Commons Attribution License (CC BY). The use, distribution or reproduction in other forums is permitted, provided the original author(s) and the copyright owner(s) are credited and that the original publication in this journal is cited, in accordance with accepted academic practice. No use, distribution or reproduction is permitted which does not comply with these terms

tape result in the highest increase in the Nusselt number of 76.27% because they form strong vortices at their geometric angles, whereas circular perforations on a single twisted tape yield the highest PEC of 1.25 due to providing smoother flow characteristics [13]. Circular perforations on multi-blade turbulators have been reported to reduce the Nusselt number by up to 15.24% compared to unperforated multi-blade configurations, while in the 8-blade configuration, the increase in frictional resistance still leads to a decrease in thermal-hydraulic performance [14].

Previous research has modified the twisting tape, ranging from comparing the perforation shapes on a single twisted tape separately to adding circular perforations on a multi-blade twisted tape to enhance heat transfer and reduce the friction factor. However, the perforation modifications on the multi-blade have not fully addressed the hydraulic penalty, especially in the 8-blade configuration. Unlike previous research, this study proposes alternating circular and hexagonal perforations (Circular–Hexagonal, Circular–Hexagonal) on multi-blade twisted tape with N = 2, 4, 6, and 8. The hexagonal angles are designed to trigger local turbulence that enhances the Nusselt number, while the circular holes serve as bypass paths that limit the friction factor. By relying on numerical analysis of Computational Fluid Dynamics (CFD), this research uses the Performance Evaluation Criteria (PEC) as the main indicator to formulate an ideal, efficient, and ready-to-apply heat exchanger configuration for the modern industrial sector.

METHODS

A. Geometry Modeling

The 3D geometry modeling is built using CAD software to facilitate the needs of computational fluid dynamics simulation. This geometric structure separates the fluid domain from the solid body. The fluid domain area is within a horizontal pipe with a diameter of 17 mm and an overall length of 1800 mm, while the Solid Body represents a twisted tape made of Stainless Steel 304. To reduce the entrance effect and stabilize the flow profile, the pipe is divided into three operational zones, including the fluid development pipe and exit pipe as calming zones, each 400 mm long, and a test pipe 1000 mm long positioned in the middle with a constant heat flux exposure of 1200 W/m². Specifically, in the test pipe section, a twisted tape 1000 mm long with a thickness of 1 mm, a width of 16 mm, and a twist ratio of y/w = 4 is placed. This research was conducted on Multi Blade twisted tape with different numbers of blades (2, 4, 6, 8) as shown in figure 2a. Each number of blades has 3 variations as shown in figure 2b, namely with Multi Blade Twisted Tape circular perforation (MBTT-C), Multi Blade Twisted Tape hexagonal perforation (MBTT-H), and Multi Blade Twisted Tape perforation circular – hexagonal (MBTT-C-H). This geometric layout generally refers to Figure 1, and details for size information on the plain tube, multiblade twisted tape, and perforations can be reviewed in Table 1.

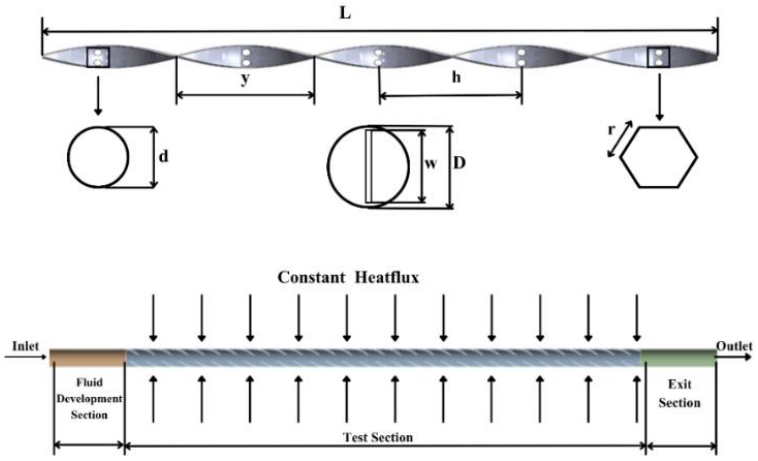


Figure 1. Geometry detail

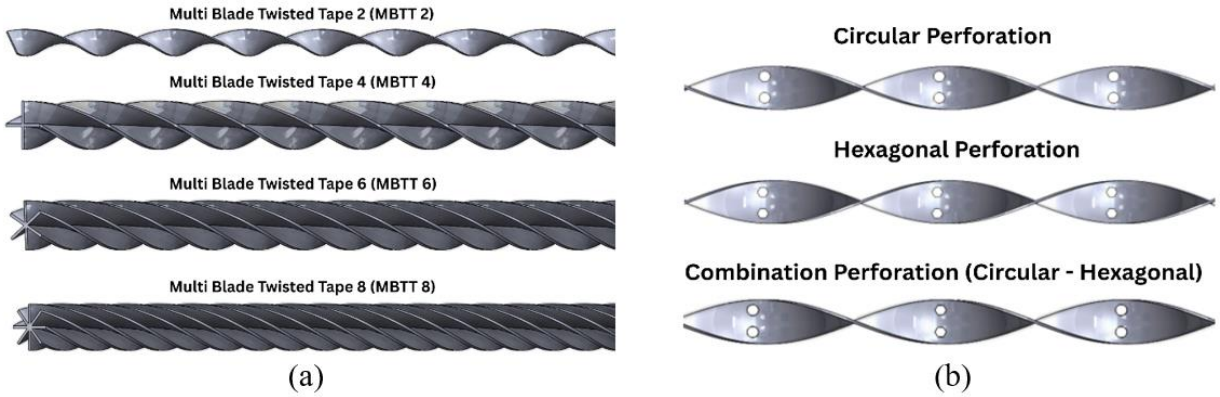


Figure 2 (a) Multi blade twisted tape configuration, (b) Perforation type

Table 1. Size details of the plain tube geometry, multi-blade twisted tape, and perforation geometry dimensions

Parameter	Description
Long Of the Twisted Tape (L)	1000 mm
Width The Twisted Tape (W)	16 mm
Diameter Circular (d)	4 mm
Hexagonal Radius (r)	2 mm
Diameter Of the tube (D)	17 mm
Pitch Twisted Tape (y)	64 mm
Distance of the perforation (h)	32 mm

B. Mesh Independent Test

In this study, the meshing process was carried out after the geometry creation. The mesh generation process in the numerical domain is carried out using tetrahedral-shaped elements as shown in Figure 3. The inflation layer with an estimated Y+ value of 1 is specifically applied in the area near the tube wall to accurately predict the turbulent flow characteristics in the boundary layer. In this study, a mesh independent test was conducted to ensure that the simulation results were independent of the number of mesh elements used. The independent mesh test was conducted with 4 variations in the number of elements, starting from 834,293, 1,140,557, 2,628,379, and 3,175,136. Figure 4 shows the trend graph results, and Table 2 shows the error results from each test. The smallest error results in this independent mesh test were 0.1% and 0.6%, which were found in the variations of 2,628,379 and 3,175,136. To shorten the simulation time, the mesh size of 2,628,379 will be used for the next tests in the research.

Table 2. Elements for mesh independent test

Number Of Element	Nu	Error
834.293	162,20	
1.140.557	159,29	2%
2.628.379	158,86	0,1%
3.175.136	157,86	0,6%

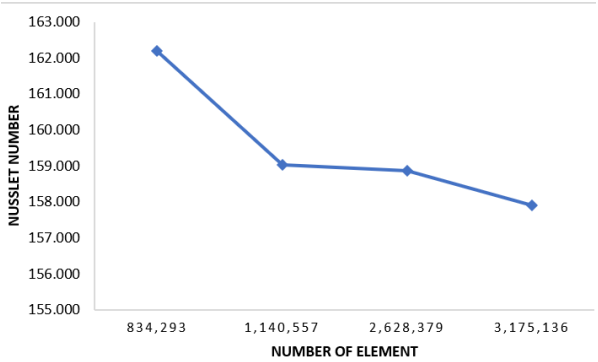


Figure 3. Mesh independent test trend graph

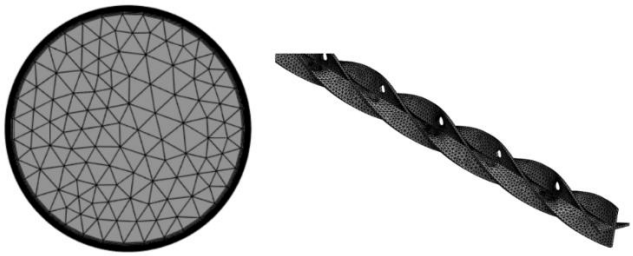


Figure 4. Plain tube mesh and mesh on multiblade twisted tape

C. Boundary Conditions and Numerical Method

The boundary condition in this numerical simulation is determined in such a way as to approximate the real working conditions of the heat exchanger. The simulation is conducted on water fluid with thermophysical properties: Density 998.2 kg/m3, Specific heat 4182 J/kg·K, Thermal conductivity 0.6 W/m·K, Dynamic viscosity 0.001003 kg/m·s. The inlet velocity used in this study is calculated based on the Reynolds number using equation (7) to first determine the hydraulic diameter and equation (8) to determine the Reynolds number. For details on the velocity and Reynolds number, please refer to Table 3.The fluid temperature at the inlet pipe is 293.15 K and the pressure condition at the outlet pipe is (gauge pressure of 0 Pa). Constant heat flux of 1200 W/m² is applied to the test pipe wall. The pipe and twisted tape are conditioned as no-slip, and the material used is stainless steel 304 with the following material properties: Density 7954.3 kg/m³, Thermal conductivity 14.924 W/m·K, Specific heat 473.62 J/kg·K.

Reynold Number:

$$Re = \frac{\rho V D_h}{\mu} \quad (7)$$

Diameter Hydraulic:

$$D_h = \frac{4A}{P} \quad (8)$$

Table 3. Boundary condition

Reynold Number	Velocity Inlet	Diameter Hydraulic
6000	0.3546 m/s	0.017 m
14000	0.8274 m/s	0.017 m
22000	1.3003 m/s	0.017 m

In this study, the research was conducted using ANSYS 2023 R1 software with a steady-state setup, employing the viscous SST k ω model. The viscous SST k ω model was specifically chosen due to its superior ability to predict complex swirl flows while capturing the effects of the viscous sublayer around the tube wall and turbulator [15], [16]. To address the coupling between pressure and velocity, the SIMPLE algorithm is integrated into the solver system. All convective terms in the momentum and energy equations are discretized using a second order upwind spatial scheme to minimize numerical errors. The convergence levels of the continuity residual, velocity components, turbulent kinetic energy, and specific dissipation rates are below 10^{-5}, and the energy equation criteria meet the

minimum threshold of 10^{-7}. TThe governing equations solved by Fluent include the continuity, momentum, energy, turbulent kinetic energy, and specific dissipation rate equations, as presented in Equations (9) – (13).

Continuity :

$$\frac{\partial \rho}{\partial t} + \nabla \cdot (\rho \boldsymbol{u}) = 0 \tag{9}$$

Momentum:

$$\rho \left(\frac{\partial \boldsymbol{u}}{\partial t} + \boldsymbol{u} \cdot \nabla \boldsymbol{u} \right) = -\nabla p + \mu \nabla^2 \boldsymbol{u} + \nabla \boldsymbol{\sigma}_\tau \tag{10}$$

Energy :

$$\frac{\partial T}{\partial t} + \nabla \cdot (\boldsymbol{u} T) = \frac{k}{\rho C_p} \nabla^2 T \tag{11}$$

Turbulent Kinetic Energy

$$\frac{\partial (\rho k)}{\partial t} + \nabla \cdot (\rho k \boldsymbol{u}) = P_k - \beta^* \rho k \omega + \nabla \cdot \left[\left(\mu + \frac{\mu_t}{\sigma_k} \right) \nabla k \right] \tag{12}$$

Specific Dissipation Rate:

$$\frac{\partial (\rho \omega)}{\partial t} + \nabla \cdot (\rho \omega \boldsymbol{u}) = \alpha \frac{\omega}{k} P_k - \beta \rho \omega^2 + \nabla \cdot \left[\left(\mu + \frac{\mu_t}{\sigma_\omega} \right) \nabla \omega \right] \tag{13}$$

D. Non-Dimensional Numbers

This research is directed to evaluate the thermal and hydraulic performance characteristics of all MBTT configurations quantitatively, ranging from heat transfer capability, flow resistance, to overall efficiency as the basis for determining the optimal configuration. Nusselt Number (Nu) is calculated using Equation (14) to show the intensity of convective heat transfer, with the convection coefficient (h) obtained through Equation (15). The friction factor (f) is calculated using Equation (16) to measure the magnitude of hydraulic resistance due to the insertion of twisted tape. Next, the overall hydraulic thermal performance is evaluated through the Performance Evaluation Criterion (PEC) in Equation (17), which compares the Nusselt Number ratio to the friction factor ratio raised to the power of 1/3 against the plain tube condition as the baseline.

$$Nu = \frac{D.h}{k} \tag{14}$$

$$h = q\ /(T_W - T_f) \tag{15}$$

$$f = \frac{\Delta P}{\left(\frac{L}{d}\right)\left(\frac{\rho . u^2}{2}\right)} \tag{16}$$

$$PEC = \frac{\left(\frac{Nu}{Nu_p}\right)}{\left(\frac{f}{f_p}\right)^{\frac{1}{3}}} \tag{17}$$

E. Validation

Validation was conducted in the research before data collection using the geometry with modified configurations. Validation in this research was conducted twice. In the initial stage, validation was performed on a smooth plain tube by comparing the Nusselt number with the Dittus-Boelter equation [17], which can be seen in equation (18), and the friction factor with the Blasius equation [18], which can be seen in equation (19). This is done to ensure the accuracy of the numerical method, such as the boundary condition and mesh arrangement, are accurate. Next, in the second validation, a case of a tube with a conventional twisted tape insert was conducted by comparing the results with experimental data from the literature. The purpose of this experimental validation is to confirm the robustness of the chosen turbulence model in predicting swirl flow phenomena and boundary layer separation with precision.

$$\mathrm{Nu} = 0.023\mathrm{Re}^{0.8}\mathrm{Pr}^{\mathrm{n}} \tag{18}$$

$$\mathrm{f} = 0.316\mathrm{Re}^{-0.25} \tag{19}$$

In Figure 5 of this initial testing phase, a deviation error of 3.83% was obtained for the Nusselt number of the plain tube compared to the Dittus Boelter correlation, and a deviation of 2.08% for the friction factor compared to the Blasius equation. Both percentage deviation errors are very small and well below the reasonable tolerance limit of < 10%, indicating that this basic smooth plain tube model is very accurate and valid. In the second validation phase, the

testing results of the twisted tape pipe with the experimental journal [12] showed a deviation error of 4.3% for the Nusselt number and 3.2% for the friction factor.

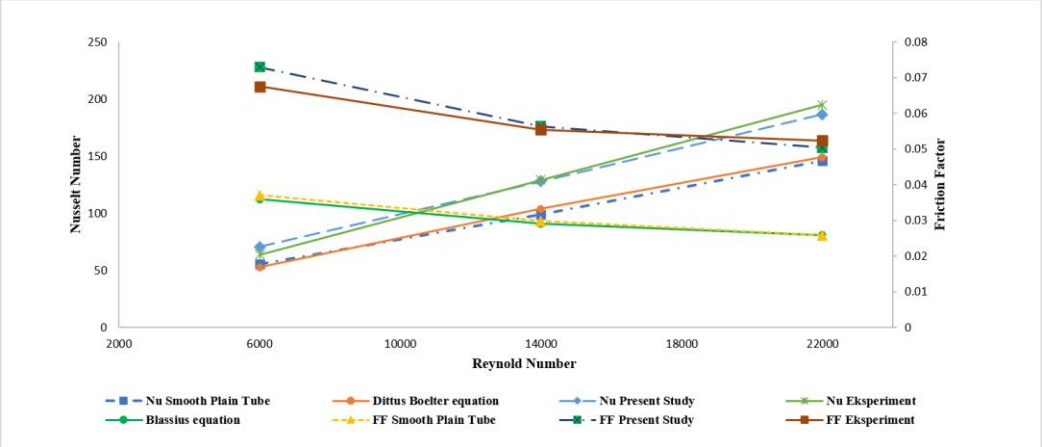


Figure 5. Validation nusselt number and friction factor

RESULT AND DISCUSSION

A. Nusselt Number

Figures 6 (a) – (d) show that all multi-blade twisted tape (MBTT) configurations are capable of increasing the Nusselt number compared to a plain tube, with values continuously increasing as the Reynolds number rises due to the thinning of the thermal boundary layer and the enhancement of convective heat transfer [19]. In addition to the influence of the Reynolds number, the increase in heat transfer is also closely related to the changes in flow structure produced by the twisted tape and the perforation geometry. Twisted tape generates swirl flow and secondary flow, while the edges of the perforations trigger local acceleration, flow separation, and vortex formation that enhance the mixing between the cooler fluid in the core region and the warmer fluid near the wall, thereby inhibiting the development of the thermal boundary layer and maintaining a higher temperature gradient near the wall. In the configuration without perforation, the increase in the number of blades from MBTT 2 to MBTT 6 strengthens the swirl flow and secondary flow due to the increased interaction between the fluid and the surface of the twisted tape, resulting in MBTT 6 producing a Nusselt number of 239.99, an increase of 80.5% compared to the plain tube. However, the increase to MBTT 8 causes a decrease in the Nusselt number because the narrower gaps between the blades increase blockage and make the vortex interaction more complex, resulting in some turbulent energy being dissipated and fluid mixing becoming less effective. In the circular perforation configuration, MBTT 6-C resulted in a 79.9% increase in the Nusselt number, which is related to the presence of a local flow resembling a jet through the circular holes, thereby enhancing fluid exchange across the twisted tape and strengthening mixing. Meanwhile, the hexagonal perforation provides the highest increase through MBTT 6-H of 82.0%, as the angles and edges of the hexagon generate stronger flow separation and vortex formation, thereby enhancing secondary flow and thermal mixing near the wall. Unlike the individual configurations, the circular-hexagonal combination shows an increase in the Nusselt number up to MBTT 8-C-H with an increase of about 76.7%, because the circular holes provide an additional path for fluid exchange, while the hexagonal holes maintain flow disruption through flow separation and vortex formation. The combination of these two mechanisms allows the enhancement of heat transfer to be maintained at a higher number of blades, although the maximum overall Nusselt number is still obtained at MBTT 6-H. This result indicates that the increase in the Nusselt number is not only determined by the number of blades or the presence of perforations, but by the interaction between blade density and perforation geometry in generating secondary flow, vortex induced mixing, and disturbances to the thermal boundary layer.

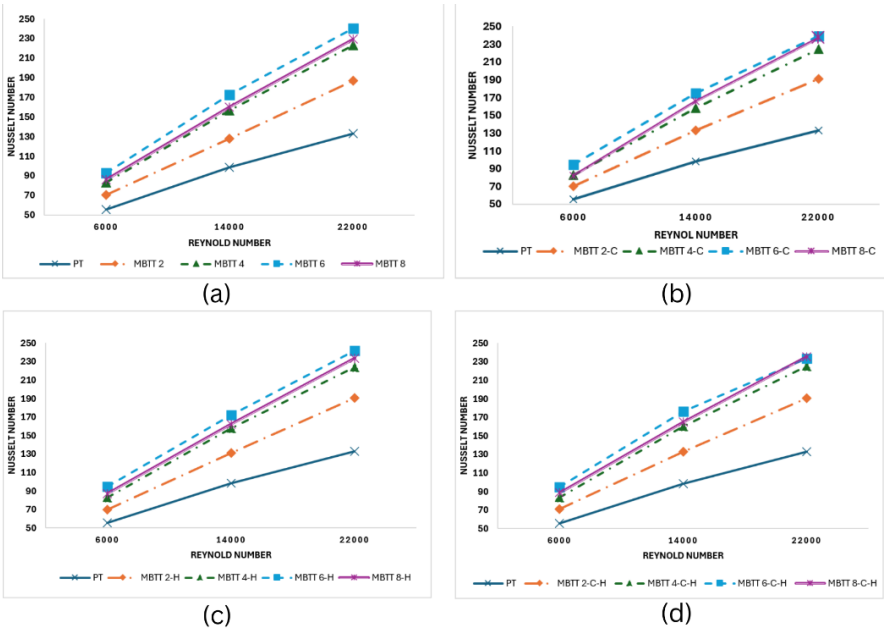


Figure 6. (a) Nusselt number graph MBTT, (b) Nusselt number graph MBTT-C, (c) Nusselt number graph MBTT-H, (d) Nusselt number graph MBTT-C-H

B. Friction Factor

Figures 7 (a) – (d) show that all multi-blade twisted tape (MBTT) configurations produce a higher friction factor compared to the plain tube, while the value decreases with increasing Reynolds number because the relative contribution of viscous forces to flow resistance becomes smaller compared to the inertia effect. In the non-perforated configuration, the friction factor increases from MBTT 2 to MBTT 8 due to the stronger swirl flow and greater blockage caused by the increased number of blades, resulting in greater fluid interaction with the twisted tape surface and increased momentum loss. Perforation changes the flow characteristics by providing additional pathways and generating flow separation and local vortices around the hole edges. At Re=22,000, MBTT 2-H produced the lowest friction factor of 0.0492, followed by MBTT 2-C-H at 0.0521 and MBTT 2-C at 0.0574. In MBTT 6, the MBTT 6-C-H configuration produced the lowest friction factor of 0.1356 compared to MBTT 6-C at 0.1773 and MBTT 6-H at 0.1593. In MBTT 6-C-H, circular perforation provides an additional path that can reduce effective blockage, while hexagonal perforation causes flow redistribution and local flow separation that maintains secondary flow. The combination of these mechanisms enhances fluid mixing and brings the core fluid close to the wall, thereby disturbing the thermal boundary layer and increasing convective heat transfer, but at the same time causing additional momentum loss reflected in the friction factor and pressure drop. In MBTT 8-C, MBTT 8-H, and MBTT 8-C-H, the friction factor becomes relatively similar in the range of 0.230–0.233 and slightly higher compared to MBTT 8 without perforation. With a high number of blades, the increasingly narrow gaps between the blades strengthen the blockage, while the vortices formed around the perforations interact with the swirl flow, increasing flow separation and momentum dissipation. As a result, the additional secondary flow that can disrupt the thermal boundary layer no longer provides a proportional hydraulic advantage, so the increase in heat transfer must be accompanied by a greater pressure loss. Thus, the effect of perforation on the friction factor is the result of the interaction between the perforation geometry, vortex formation, secondary flow, and blockage, where certain configurations can maintain the disturbance of the thermal boundary layer to enhance heat transfer, but the increased intensity of flow disturbance also results in a hydraulic penalty that subsequently affects the PEC value.

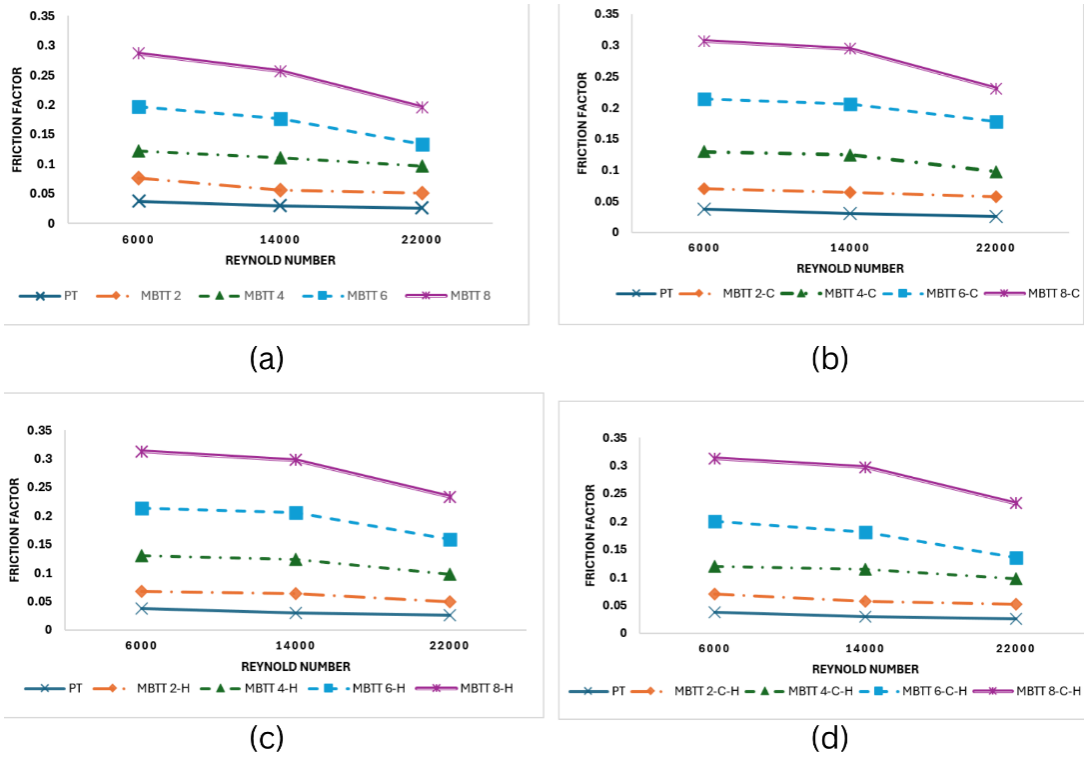


Figure 7. (a) Friction factor graph MBTT, (b) Friction factor graph MBTT-C, (c) Friction factor graph MBTT-H, (d) Friction factor graph MBTT-C-H

C. Pressure Drop

Figures 8 (a) – (d) show that the pressure drop increases with the increase in Reynolds number and the number of blades. The increase in Reynolds number enhances the flow momentum, making the interaction between the fluid and the twisted tape and the channel wall stronger, while the addition of blades narrows the flow path and increases hydraulic resistance. At Re=22,000, the pressure drop increased from 2,653 Pa at MBTT 2 to 5,115 Pa at MBTT 4, 6,999 Pa at MBTT 6, and 10,309 Pa at MBTT 8. The differences due to perforation began to be noticeable at the medium number of blades, especially at MBTT 6, where MBTT 6-C-H resulted in a pressure drop of 7,139 Pa, lower than MBTT 6-H at 8,391 Pa and MBTT 6-C at 9,336 Pa, although still slightly higher than MBTT 6 without perforation. This condition indicates that the circular-hexagonal combination can alter the flow distribution around the twisted tape; some fluid can pass through the circular perforations, while the hexagonal shape provides local disturbances that maintain the formation of secondary flow. These path changes can enhance fluid mixing and disrupt the thermal boundary layer near the wall, thereby supporting heat transfer, but still cause pressure loss due to flow direction changes and flow separation around the perforations. In MBTT 8, the effect becomes less favorable as the pressure drop increases to 12,142 Pa in MBTT 8-C, 12,279 Pa in MBTT 8-H, and 12,246 Pa in MBTT 8-C-H, compared to 10,309 Pa in MBTT 8 without perforation. At high blade density, the increasingly limited flow space causes blockage to become the dominant factor, while the interaction between vortical structures around the perforation and swirl flow amplifies flow separation and momentum dissipation. As a result, the increase in secondary flow that has the potential to enhance thermal boundary layer disturbances is no longer proportional to the additional hydraulic loss. These results indicate that perforation not only serves as an additional pathway for flow but also alters the flow structure and the balance between thermal mixing and pressure loss; these conditions are further reflected in changes in the friction factor and determine the magnitude of thermal-hydraulic performance through PEC.

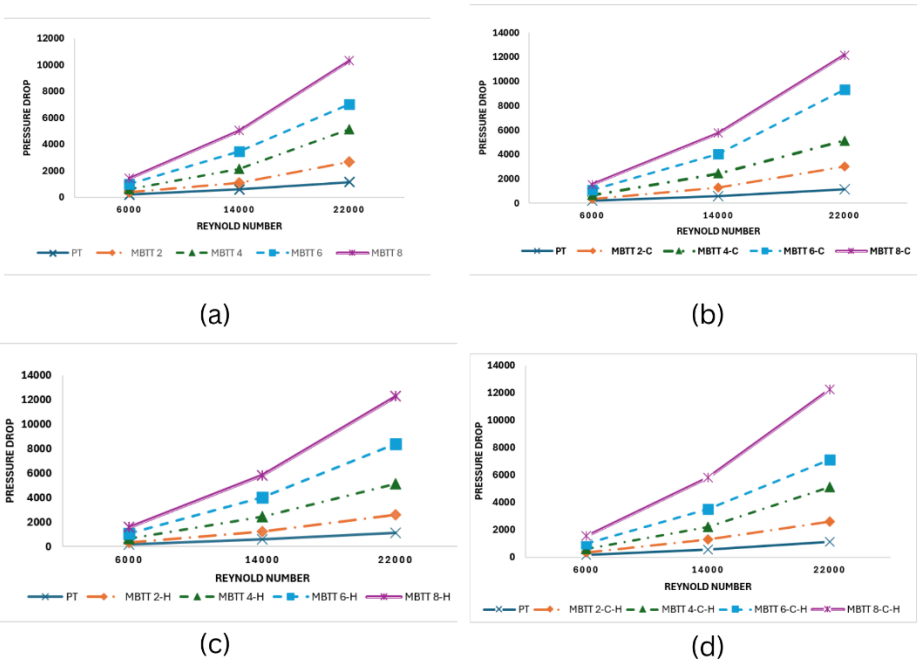


Figure 8. (a) Pressure drop graph MBTT, (b) Pressure drop graph MBTT-C, (c) Pressure drop graph MBTT-H, (d Pressure drop graph MBTT-C-H

D. Performance Evaluation Criterion (PEC)

Figures 9 (a) – (d) show that the Performance Evaluation Criterion (PEC) value tends to decrease as the number of blades increases because the increase in heat transfer is no longer proportional to the increase in friction factor and pressure loss [20]. The flow passing through the twisted tape experiences a change in direction and rotational movement, forming a secondary flow that carries the fluid from the core region to the wall and disrupts the thermal boundary layer, while perforation alters the flow distribution by creating additional pathways, flow separation, and local vortices around the hole edges. At Re=22,000, MBTT 2-C-H produced a PEC of 1.136, higher than MBTT 2-C at 1.101, MBTT 2-H at 1.128, and MBTT 2 at 1.125. This condition is related to the combination of circular and hexagonal perforation characteristics, where the circular holes provide additional pathways that can reduce effective blockage, while the sides and angles of the hexagonal holes create local disturbances that enhance flow redistribution and vortex formation. That interaction enhances the mixing between the core flow and the region near the wall, thereby disturbing the thermal boundary layer more and potentially increasing heat transfer. However, the formation of vortices and changes in flow direction also increase momentum loss due to friction and flow separation. When the number of blades is increased to MBTT 8, the flow space becomes narrower, resulting in stronger blockage and interaction between the vortices around the perforation and the swirl flow. This is reflected in the PEC values of MBTT 8-C-H at 0.851, MBTT 8-H at 0.844, MBTT 8-C at 0.842, and MBTT 8 at 0.848. Although the C-H configuration still yields slightly higher values, all values are below one because the increase in heat transfer has not been able to compensate for the hydraulic penalty due to the increasing friction factor and pressure drop. The results indicate that the influence of perforation on thermal-hydraulic performance is not only determined by the ability of the holes to provide additional flow paths but also by the interaction between perforation geometry, flow separation, vortex formation, secondary flow, thermal boundary layer disturbance, and pressure loss. Thus, configurations with a higher Nusselt number do not always result in a higher PEC because the increase in heat transfer must be considered alongside the energy required to maintain the flow through the twisted tape.

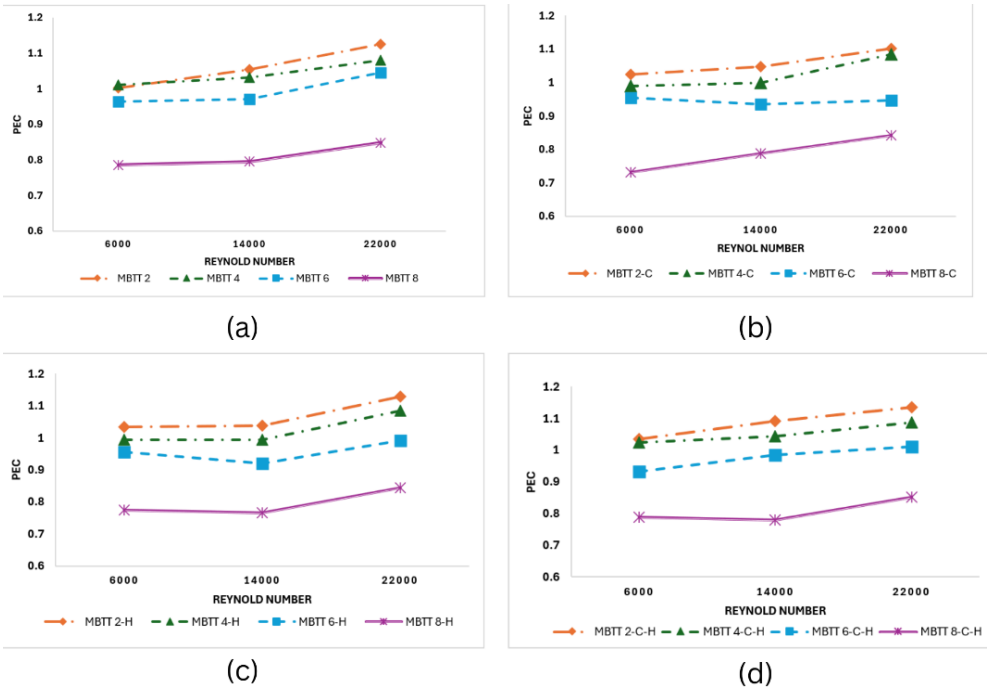


Figure 9. (a) Performance Evaluation Criterion graph MBTT, (b) Performance Evaluation Criterion graph MBTT-C, (c) Performance Evaluation Criterion graph MBTT-H, (d) Performance Evaluation Criterion graph MBTT-C-H

E. Temperature contour

Figure 10 shows the temperature contours on the cross-section of the tube for the plain tube, MBTT 6, MBTT 6-H, MBTT 8, and MBTT 8-C-H at Re=22,000. In the plain tube, relatively low temperatures still dominate the core flow region and increase toward the heated wall, forming a thermal boundary layer between the wall surface and the core flow. The significant temperature difference between the two regions indicates that the heat received by the fluid is still concentrated around the wall, resulting in an suboptimal distribution of thermal energy toward the core section. After MBTT 6 was installed, the temperature transition area from the wall to the center of the tube appeared wider. This condition indicates that heat from the wall can be distributed further into the fluid, thereby reducing the thermal resistance near the wall and making convective heat transfer more effective. In MBTT 6-H, the temperature distribution pattern is still relatively similar to MBTT 6, but local changes are observed in the area around the perforation. These changes indicate that the presence of perforations affects the temperature distribution on the cross-section and causes the heat energy to spread with different characteristics compared to twisted tape without perforations [13]. In the MBTT 8 configuration, areas with higher temperatures are still concentrated around the walls, and the temperature distribution appears less uniform compared to the MBTT 6 configuration. This condition indicates that the addition of blade numbers does not always result in a proportional increase in heat transfer, as the development of the thermal boundary layer and the distribution of thermal energy in the wall-adjacent region remain important factors in the heat transfer process. These results are consistent with the trend of the Nusselt number in MBTT 8, which shows that increasing the number of blades without perforation does not provide a proportional increase in heat transfer. On the other hand, in MBTT 8-C-H, the temperature distribution appears to be more spread out from the wall region toward the core compared to MBTT 8. These conditions indicate that the combination of circular-hexagonal perforations can modify the temperature distribution and reduce the heat concentration around the wall. The more effective dispersion of thermal energy indicates that the thermal boundary layer experiences greater disturbance, thereby reducing the thermal resistance between the wall and the core fluid. As a result, heat from the tube surface can be transferred more effectively to the fluid and supports improved heat transfer performance in the MBTT 8-C-H configuration [14].

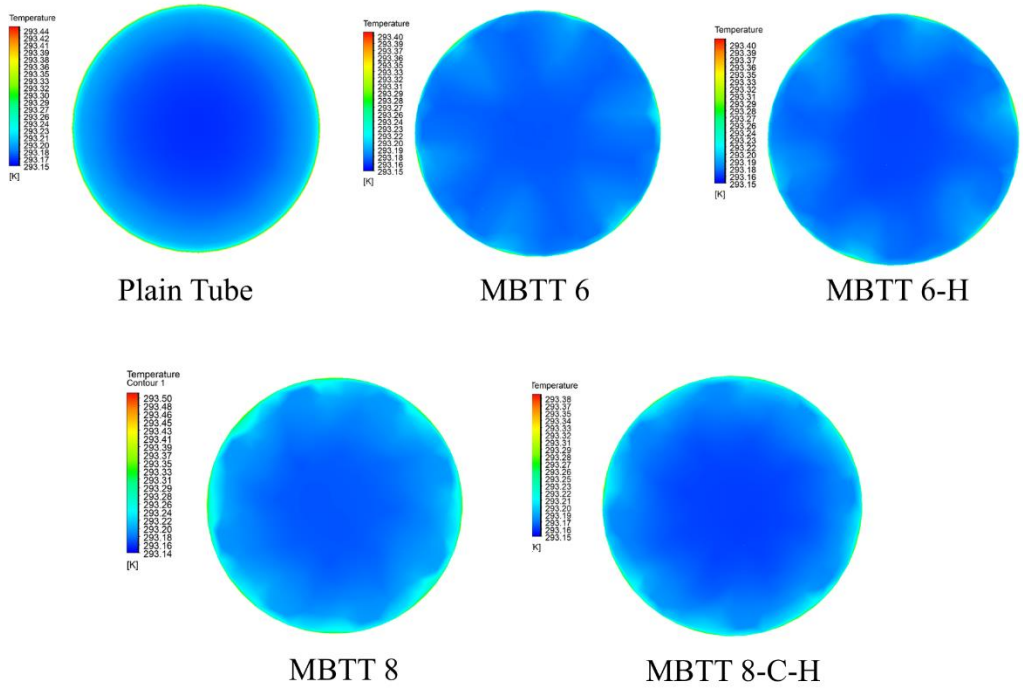


Figure 10. Temperature Contour at Re = 22.000 and a distance of 900 mm from the inlet.

F. Velocity Contour

Figure 10 shows the velocity contours on the cross-section of the tube for the plain tube, MBTT 6, MBTT 6-H, MBTT 8, and MBTT 8-C-H at Re=22,000. In the plain tube, the maximum velocity reaches 1.49 m/s in the core region and decreases toward the wall due to the no-slip condition. This distribution indicates that the fluid transfer from the core to the wall is still limited, allowing the thermal boundary layer to develop near the heating surface. In the MBTT 6, a high-velocity zone is formed between the blades with a maximum velocity of 2.03 m/s, while lower velocities are observed around the surface of the twisted tape. The narrowing of the flow path causes local acceleration and changes in the velocity distribution that support transverse fluid transfer, thereby disturbing the thermal boundary layer more and increasing heat transfer. In MBTT 6-H, the maximum velocity increased to 2.07 m/s. Hexagonal perforation provides an additional path for some of the fluid to pass through the twisted tape and generates a change in velocity around the edge of the hole. This condition can trigger flow separation and local vortex structures that aid in fluid mixing, although the change in flow direction also adds to momentum loss. In MBTT 8, the larger number of blades constricts the flow space and increases flow blockage. The maximum velocity in the displayed field is only 1.41 m/s, with a more dominant low-velocity area. These conditions indicate that an increase in the number of blades does not always result in a more effective flow distribution, while fluid interaction with the twisted tape increases the hydraulic penalty. Conversely, MBTT 8-C-H achieves a maximum speed of 2.26 m/s with a more distinct high-speed zone. Circular and hexagonal perforations provide additional pathways for the flow, resulting in a more dispersed velocity distribution while maintaining flow disturbance. This condition helps disrupt the thermal boundary layer and supports the enhancement of heat transfer. However, the increase in local velocity is still accompanied by momentum loss due to friction, changes in flow direction, and disturbances around the perforation. Thus, the impact of perforation on thermal-hydraulic performance is determined by the balance between changes in flow distribution, disruption of the thermal boundary layer, enhancement of heat transfer, and hydraulic penalty.

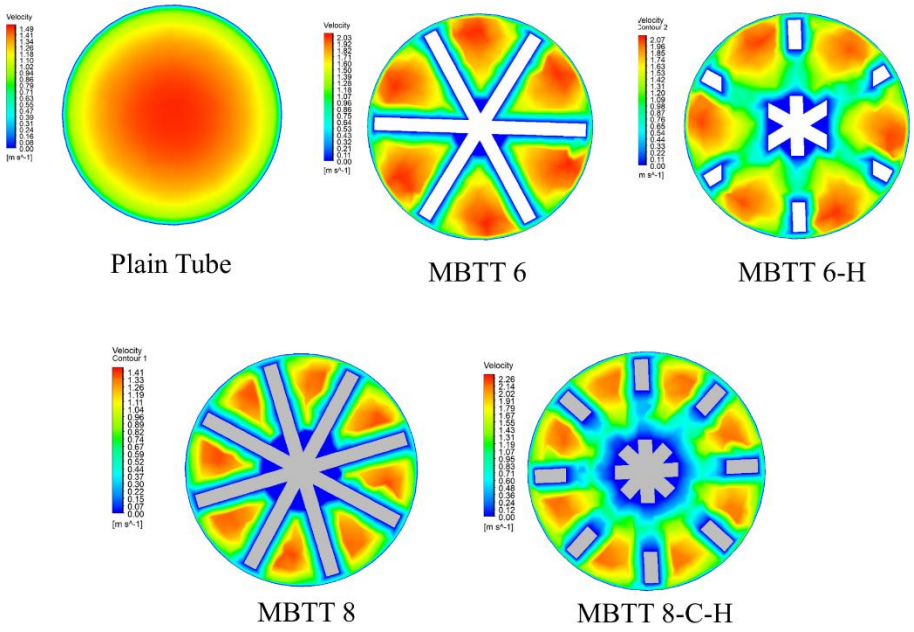


Figure 11. Velocity Contour at Re = 22.000 and a distance of 900 mm from the inlet.

CONCLUSION

The use of multi-blade twisted tape (MBTT) enhances heat transfer compared to a plain tube, with a maximum Nusselt number increase of 82.0% obtained with MBTT 6-H at Re=22,000. The maximum PEC value of 1.136 was obtained with MBTT 2-C-H at Re=22,000. The increase in the number of blades raises the hydraulic penalty, with the pressure drop increasing from 2,653 Pa in the MBTT 2 to 10,309 Pa in the MBTT 8. In the MBTT 6 with perforation, the MBTT 6-C-H configuration produces the lowest pressure drop of 7,139 Pa compared to other MBTT 6 perforation configurations. In the eight blade configuration, the PEC value ranges from 0.842 to 0.851, indicating that the increase in heat transfer has not yet been able to offset the increase in hydraulic resistance. Overall, the alternating circular–hexagonal perforation configuration shows a PEC value above one at lower blade counts, while the increase in hydraulic penalty becomes more dominant at higher blade counts. Further research can be focused on variations in size and perforation patterns, as well as experimental validation to evaluate the application of these configurations in heat exchanger systems.

REFERENCE

[1] M. Omidi, M. Farhadi, and M. Jafari, “A comprehensive review on double pipe heat exchangers,” Jan. 05, 2017, *Elsevier Ltd*. doi: 10.1016/j.applthermaleng.2016.09.027.

[2] M. Paikar, K. Hosseinzadeh, J. R. Kermani, and D. D. Ganji, “Hydrothermal assessment of a double-pass shell and tube heat exchanger in the presence of blade turbulators with different configurations,” *International Journal of Thermofluids*, vol. 21, Feb. 2024, doi: 10.1016/j.ijft.2024.100577.

[3] T. L. . Bergman and A. S. . Levine, *Fundamentals of heat and mass transfer*. John Wiley & Sons, Inc., 2019.

[4] M. Okiishi and H. Rothmayer, “Fundamentals of Fluid seventh edition Mechanics,” 2013.

[5] Varun, M. O. Garg, H. Nautiyal, S. Khurana, and M. K. Shukla, “Heat transfer augmentation using twisted tape inserts: A review,” Sep. 01, 2016, *Elsevier Ltd*. doi: 10.1016/j.rser.2016.04.051.

[6] M. M. K. Bhuiya, A. K. Azad, M. S. U. Chowdhury, and M. Saha, “Heat transfer augmentation in a circular tube with perforated double counter twisted tape inserts,” *International Communications in Heat and Mass Transfer*, vol. 74, pp. 18–26, May 2016, doi: 10.1016/j.icheatmasstransfer.2016.03.001.

[7] T. Alam and M. H. Kim, “A critical review on artificial roughness provided in rectangular solar air heater duct,” Mar. 01, 2017, *Elsevier Ltd*. doi: 10.1016/j.rser.2016.11.192.

[8] W. He, D. Toghraie, A. Lotfipour, F. Pourfattah, A. Karimipour, and M. Afrand, “Effect of twisted-tape inserts and nanofluid on flow field and heat transfer characteristics in a tube,” *International Communications in Heat and Mass Transfer*, vol. 110, Jan. 2020, doi: 10.1016/j.icheatmasstransfer.2019.104440.

[9] A. Kahsay Kiros, D. Goytom Tewolde, A. Kidanu Atsbeha, K. Gebremicheal Gebru, and T. Tekleab Teklehaimanot, “Effect of multi-leg twisted tape inserts on heat transfer and pressure drop characteristics of a laminar pipe flow: A comparative analysis,” *Case Studies in Thermal Engineering*, vol. 74, p. 106838, Oct. 2025, doi: 10.1016/j.csite.2025.106838.

[10] Y. Ju *et al.*, "Evaluation of multiple semi-twisted tape inserts in a heat exchanger pipe using al2o3 nanofluid," *Nanomaterials*, vol. 11, no. 6, Jun. 2021, doi: 10.3390/nano11061570.
[11] A. Saysroy and S. Eiamsa-ard, "Enhancing convective heat transfer in laminar and turbulent flow regions using multi-channel twisted tape inserts," *International Journal of Thermal Sciences*, vol. 121, pp. 55–74, Nov. 2017, doi: 10.1016/j.ijthermalsci.2017.07.002.
[12] T. Dagdevir and V. Ozceyhan, "An experimental study on heat transfer enhancement and flow characteristics of a tube with plain, perforated and dimpled twisted tape inserts," *International Journal of Thermal Sciences*, vol. 159, Jan. 2021, doi: 10.1016/j.ijthermalsci.2020.106564.
[13] A. Bouregueba, A. Begag, R. Saim, and M. A. Kherrafi, "Heat Transfer Enhancement in a Heat Exchanger Tube Using Twisted Tapes with Circular and Hexagonal Perforations," *International Journal of Thermodynamics*, vol. 28, no. 3, pp. 176–186, 2025, doi: 10.5541/ijot.1653747.
[14] R. Sedaghat, K. Mobarhan Dalili, and S. M. Hosseinalipour, "A comprehensive analysis of heat transfer in a heat exchanger with simple and perforated twisted tapes based on numerical simulations," *Case Studies in Thermal Engineering*, vol. 56, Apr. 2024, doi: 10.1016/j.csite.2024.104227.
[15] R. Cabello, A. E. Plesu Popescu, J. Bonet-Ruiz, D. Curcó Cantarell, and J. Llorens, "Heat transfer in pipes with twisted tapes: CFD simulations and validation," *Comput. Chem. Eng.*, vol. 166, Oct. 2022, doi: 10.1016/j.compchemeng.2022.107971.
[16] K. L. Liaw, J. C. Kurnia, and A. P. Sasmito, "Turbulent convective heat transfer in helical tube with twisted tape insert," *Int. J. Heat Mass Transf.*, vol. 169, Apr. 2021, doi: 10.1016/j.ijheatmasstransfer.2021.120918.
[17] F. W. Dittus, L. M. K. Boelter, and V.] 12, "HEAT TRANSFER IN AUTOMOBILE RADIATORS OF THE TUBULAR TYPE."
[18] T. Dagdevir, M. Uyanik, and V. Ozceyhan, "The experimental thermal and hydraulic performance analyses for the location of perforations and dimples on the twisted tapes in twisted tape inserted tube," *International Journal of Thermal Sciences*, vol. 167, Sep. 2021, doi: 10.1016/j.ijthermalsci.2021.107033.
[19] M. E. Nakhchi and J. A. Esfahani, "Numerical investigation of rectangular-cut twisted tape insert on performance improvement of heat exchangers," *International Journal of Thermal Sciences*, vol. 138, pp. 75–83, Apr. 2019, doi: 10.1016/j.ijthermalsci.2018.12.039.
[20] K. S. Mushatet, Q. A. Rishak, and M. H. Fagr, "Experimental and numerical investigation of swirling turbulent flow and heat transfer due to insertion of twisted tapes of new models in a heated tube," *Appl. Therm. Eng.*, vol. 171, May 2020, doi: 10.1016/j.applthermaleng.2020.115070.

This page is intentionally left blank